論文97-34D-10-1

마이크로웨이브 이미징에서 위상오차 분산과 코릴레이션 계수와의 상호관계

(Interrelationship of phase-error variance and correlation coefficient in microwave imaging)

姜 鳳 淳 *, 楊 勳 其 **

(Bongsoon Kang and Hoon-Gee Yang)

요 약

본 논문은 복원 영상의 선명도에 대한 상대적 평가 척도로 많이 활용되는 correlation 계수의 최소값이 어레이 안테나에 수신된 신호의 위상오차의 분산에 의해 결정됨을 수학적으로 유도한다. adaptive beamformer로 사용되는 range bin의 위상 오차에 대한 분산값을 알고 있으면 복잡한 영상 복원과정을 거치지 않고서도 미리 복원 영상의 선명도를 예측할 수 있으며 복원 영상의 correlation 값도 항상 유도된 최소값 이상을 가짐을 보인다. 증명을 위해 실제 실험 데이터를 사용하며 adaptive beamforming 알고리듬으로 dominant scatterer algorithm (DSA)이 사용된다.

Abstract

This paper presents the theoretical derivation relating an image correlation coefficient capable of assessing image quality, with phase-error variance in antenna aperture domain. We show that when the phase-error variance of a range bin selected as an adaptive beamformer is known, the quality of the reconstructed image is predictable and moreover, the resultant correlation coefficient is obviously greater than the derived lower bound. To support the derivation, real data are used for image formation where the dominant scatterer algorithm (DSA) is applied for phase compensation.

I. Introduction

The radio camera is a high-resolution, two-dimensional microwave imaging instrument in which the distortion in its large aperture, which is usually a large phased array, is self-corrected by a process called adaptive beamforming (ABF)[1]. Its success depends upon the known properties of the reradiation from a target or scatterer having large radar cross section (RCS) and small physical size. The aforementioned self-correcting procedure is called the dominant scatterer algorithm (DSA). The basic procedure for the DSA assumes that there exists somewhere in the field of view of the imaging system a point-like scatterer or source having large radar cross section or source strength[2],[3]. A corner reflector proves to be an excellent target for the beamforming procedure. The theory governing the requirements on its characteristics is given in

* 正會員, System LSI, 三星電子
(System LSI, Samsung Electronics)
** 正會員, 光云大學校 電波工學科 新技術研究所
(Dept. of Radio Science & Eng., Institute of New Technology, Kwangwoon Univ.)
接受日字:1997年7月19日, 수정완료일:1997年9月18日

[4]. It was shown that the physical size of the source can be no larger than $\lambda R/2L$, where λ is the wavelength, R is the radar-to-target distance, and L is the size of the imaging aperture; and that its echo strength must exceed the total backscatterer from all the other scatterers in its range bin by at least 4 dB. Such a target or source radiates a nearly spherical wavefront, which induces a simple phase variation across the array. Provided that the array is linear or planar, the phase variation is linear if the target or the source is in the far field, or approximately quadratic when the source is in the near field. Deviations from such simple behavior indicate geometric distortion in the array, electrical mistunings, or wavefront distortion due to turbulence in the propagation medium.

While the success of the radio camera greatly depends upon the correct phase synchronization achieved by the adaptive beamforming process, phase distortions remaining even after the beamforming process are in fact unavoidable, resulting in the image degradation. In case of DSA, the proper choice of a beamforming bin has a great effect on the quality of the output image. Hence, some statistical properties of the measured signals on the antenna aperture domain were investigated to see whether it can be a valid beamforming source. Target-to-clutter ratio is one of the properties. It was shown that the beamforming bins having the target-to-clutter ratio greater than 2.5 can produce a satisfactory image[5].

In this paper, we investigate, as an another property, the phase-error variance of the beamforming bin and derive the relation between the phase-error variance and an image correlation coefficient which was considered a useful estimator of the image degradation[6].

In section II, we present the theoretical derivation. In section III, we review the procedure of the image formation. The derived relation is numerically proved with real experimental data in section IV.

II. Lower Bound of Image Correlation Coefficient

A complex radiation pattern for a discrete array is given in detail by the diffraction relation[1]. Let $g(u)$ be the complex radiation pattern steered u_o where $u_o = \sin\theta_o$ with θ_o describing the angle from the array broadside to the field point. Then, the radiation patterns in the absence and in the presence of the random phase errors are

$$g_1(u) = \frac{1}{N}\sum_{n=1}^{N} A_n e^{-jkx_n(u-u_o)} \tag{1}$$

$$g_2(u) = \frac{1}{N}\sum_{n=1}^{N} A_n e^{j\delta\phi_n} e^{-jkx_n(u-u_o)} \tag{2}$$

where x_n is the distance between the first array element and the nth array element and $k = 2\pi/\lambda$ with wavelength λ. A_n is the signal amplitude measured at the nth element and N denotes the number of the array elements. $\delta\phi_n$ represents phase errors across the distorted array. Since the measured phases of each range bin are randomly distributed over $[-\pi, \pi]$, we will consider $\delta\phi_n$ as an independent and identically distributed random variable with a Gaussian distribution having zero mean and variance $\sigma^2_{\delta\phi}$. The source distribution comprised of point targets can be written as

$$S(u) = \sum_{i=1}^{I} S_i\,\delta(u-u_i) \tag{3}$$

where S_i is the complex weight of the ith target, $u_i = \sin\theta_i$ is its angular location with θ_i describing the angle from the array broadside to the ith target, and I is the number of the targets. Then, the estimated image sets can be written in the absence and in the presence of the random phase errors as

$$\hat{S}_1(u) = S(u) * f_1(u) = \sum_{i=1}^{I} S_i\, f_1(u-u_i) \tag{4}$$

$$\hat{S}_2(u) = S(u) * f_2(u) = \sum_{i=1}^{I} S_i\, f_2(u-u_i) \tag{5}$$

where the asterisk denotes a convolution. and $f_1(u)$ and $f_2(u)$ are the radiation patterns which do not include beam steering factors in $g_1(u)$ and $g_2(u)$, respectively. For example, $f_1(u)=\frac{1}{N}\sum_{n=1}^{N} A_n e^{jkx_n u}$. The correlation coefficient ρ between two images is given in [6] as

$$\rho=\frac{E[\int_{-1}^{1}|\hat{S}_1(u)\ \hat{S}_2^*(u)|du]}{\sqrt{E[\int_{-1}^{1}|\hat{S}_1(u)|^2du]E[\int_{-1}^{1}|\hat{S}_2(u)|^2du]}} \tag{6}$$

where $|\ |$ denotes an absolute value and the superscript '*' denotes a complex conjugate. By using the Schwartz inequality [7], the expected value of the integral in the numerator can be written as

$$E[\int_{-1}^{1}|\hat{S}_1(u)\ \hat{S}_2^*(u)|du] \geq E[|\int_{-1}^{1}\hat{S}_1(u)\ \hat{S}_2^*(u)du|]$$

$$=E[|\sum_{i=1}^{I}\sum_{j=1}^{I}S_iS_j^*\int_{-1}^{1}f_1(u-u_i)f_2^*(u-u_j)du|] \tag{7}$$

where the equality holds if and only if $\hat{S}_1(u)=C\hat{S}_2(u)$, with constant C. $\int f_1(u-u_i)f_2^*(u-u_j)du$ is very small for $u_i\neq u_j$ because the radiation pattern without beam steering factor will asymptotically become $\delta(u)$ [1] when the aperture size is significantly large. Then, the integral can be written only for $u_i=u_j$ as

$$\int_{-1}^{1}f_1(u-u_i)f_2^*(u-u_j)du=\int_{-1}^{1}f_1(u)f_2^*(u)du$$

$$=\frac{1}{N^2}\sum_{m=1}^{N}\sum_{n=1}^{N}A_mA_ne^{-j\delta\phi_n}e^{jku_i(r_m-r_n)}\int_{-1}^{1}e^{-jku(r_m-r_n)}du$$

$$=\frac{1}{N^2}\sum_{m=1}^{N}A_m^2e^{-j\delta\phi_m}\delta_{m,n} \tag{8}$$

where $\int e^{-jku(r_m-r_n)}du=\delta_{m,n}$ and $\delta_{m,n}$ represents the Kronecker-Delta equal to one for $m=n$ and zero otherwise. Let's assume that all A_m are equal to one across the array. By substituting (8) into (7), we get

$$E[|\int_{-1}^{1}\hat{S}_1(u)\ \hat{S}_2^*(u)du|]=\frac{1}{N^2}\sum_{i=1}^{I}|S_i|^2\,E[|\sum_{m=1}^{N}e^{-j\delta\phi_m}|] \tag{9}$$

since $|S_i|^2=S_iS_i^*$ is real. By using sinusoidal functions to expand $e^{-j\delta\phi_m}$, the expected value in (9) can be written as

$$E[|\sum_{m=1}^{N}e^{-j\delta\phi_m}|]=E[|\sum_{m=1}^{N}\cos(\delta\phi_m)-j\sum_{m=1}^{N}\sin(\delta\phi_m)|]$$

$$=E[\sqrt{\{\sum_{m=1}^{N}\cos(\delta\phi_m)\}^2+\{\sum_{m=1}^{N}\sin(\delta\phi_m)\}^2}\ ]$$

$$=E[\sqrt{N+\sum_{m\neq}^{N}\sum_{n}^{N}\cos(\delta\phi_m-\delta\phi_n)}\ ]$$

$$=E[\sqrt{N+\sum_{m\neq}^{N}\sum_{n}^{N}\{1-\sin^2(\frac{\delta\phi_m-\delta\phi_n}{2})\}}\ ]$$

$$=E[N\sqrt{1-\frac{2}{N^2}\sum_{m\neq}^{N}\sum_{n}^{N}\sin^2(\frac{\delta\phi_m-\delta\phi_n}{2})}\ ]$$

$$=E[N-\frac{1}{2N}\sum_{m\neq}^{N}\sum_{n}^{N}\{1-\cos(\delta\phi_m-\delta\phi_n)\}\ ]$$

$$=E[N-\frac{N^2-N}{2N}+\frac{1}{4N}\sum_{m\neq}^{N}\sum_{n}^{N}\{e^{j(\delta\phi_m-\delta\phi_n)}+e^{-j(\delta\phi_m-\delta\phi_n)}\}\ ]$$

$$=\frac{N}{2}(1+e^{-\sigma_{\delta\phi}^2})+\frac{1}{2}(1-e^{-\sigma_{\delta\phi}^2}) \tag{10}$$

where $|\frac{2}{N^2}\sum_{m\neq}^{N}\sum_{n}^{N}\sin^2(\frac{\delta\phi_m-\delta\phi_n}{2})|\ll 1$, $E[e^{-j(\delta\phi_m-\delta\phi_n)}]=e^{-\sigma_{\delta\phi}^2}$ with $m\neq n$, $N^2\gg 1$, and $\cos\phi=1-2\sin^2(\phi/2)$. By substituting (10) into (9), the expression for the numerator can be written as

$$E[|\int_{-1}^{1}\hat{S}_1(u)\ \hat{S}_2^*(u)du|]=$$

$$\frac{1}{N^2}\sum_{i=1}^{I}|S_i|^2\frac{N}{2}(1+e^{-\sigma_{\delta\phi}^2})+\frac{1}{2}(1-e^{-\sigma_{\delta\phi}^2})). \tag{11}$$

The expected value in the denominator is more simply solved as

$$E[\int_{-1}^{1}|\hat{S}_1(u)|^2du]=E[\int_{-1}^{1}|\hat{S}_2(u)|^2du]$$

$$=E[\sum_{i=1}^{I}\sum_{j=1}^{I}S_iS_j^*\int_{-1}^{1}f_1(u-u_i)\,f_1^*(u-u_j)du\,]. \tag{12}$$

Since $\int f_1(u-u_i)f_1^*(u-u_j)du$ is negligible for $u_i\neq u_j$, the integral in (12) can be written only for $u_i=u_j$ as

$$\int_{-1}^{1}f_1(u-u_i)f_1^*(u-u_j)du$$

$$=\frac{1}{N^2}\sum_{m=1}^{N}\sum_{n=1}^{N}e^{jku_i(r_m-r_n)}\int_{-1}^{1}e^{-jku(r_m-r_n)}du=\frac{1}{N}. \tag{13}$$

Substitution of (13) into (12) with $u_i = u_j$ gives the solution for the denominator, i.e.,

$$E[\int_{-1}^{1}|\hat{S}_1(u)|^2du] = E[\int_{-1}^{1}|\hat{S}_2(u)|^2du] = \frac{1}{N}\sum_{i=1}^{L}|S_i|^2. \quad (14)$$

By using (6), (11), and (14), the theoretical lower bound ρ_o on the correlation coefficient in terms of phase-error variance can be derived as

$$\rho \geq \frac{1}{2}(1+e^{-\sigma_{\delta_R}^2})+\frac{1}{2N}(1-e^{-\sigma_{\delta_R}^2}) \equiv \rho_o. \quad (15)$$

(15) reveals that the lower bound of the image correlation coefficient can be represented in terms of the phase-error variance and the number of array elements. Thereby, with a priori of the phase-error variance in antenna aperture domain, one can easily guess the resulting image quality. Figure 1 depicts the lower bounds on the image correlation coefficient according to the root mean square (*rms*) phase errors and the number of antenna elements. The numbers of the elements used are 100 and 330. It shows that about 28 *rms* phase errors guarantee the correlation coefficients of 0.9. (15) also demonstrates that the smaller the phase-error variance, the higher the correlation coefficient.

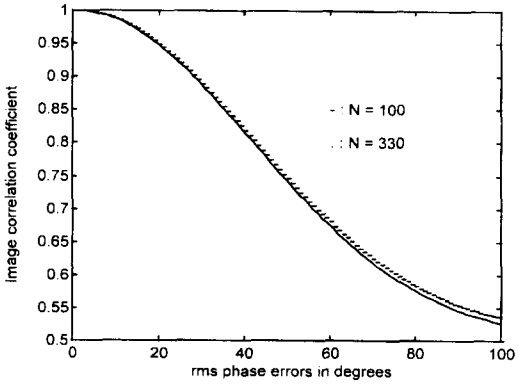

그림 1. rms 위상 오차와 element 수에 의해 주워지는 이미지 코릴레이션 계수의 최소값

Fig. 1. Lower bound of image correlation coefficients based on rms phase errors and number of array elements.

Ⅲ. Image Formation

To calculate the correlation coefficient, we need to have the images reconstructed. In this section, we briefly summarize the procedure of image formation[1]. The procedure consists of multiplication, followed by Fourier transform. The electric field $E(x)$ measured at the antenna element is

$$E(x) = F^{-1}[S(u)] \quad (16)$$

where F^{-1} denotes the inverse Fourier transform, $S(u)$ is the source distribution defined in (3) and x, the Fourier variable for ku, specifies a coordinate in the antenna aperture direction. Thus, if measured signals across the array are error-free, the image is simply reconstructed by taking Fourier transform of the measured signals. In reality, it is not the case and the antenna weight vector $w(x)$ is multiplied to the electric field to compensate phase errors, which results in the following current distribution

$$i(x) = w(x)E(x) = w(x)F^{-1}[S(u)]. \quad (17)$$

It is noted that the process to find $w(x)$ is the adaptive beamforming algorithm and in this work, we choose the DSA. The reconstructed image $\hat{S}(u)$ is obtained by taking the Fourier transform of $i(x)$, i.e.,

$$\hat{S}(u) = F[w(x)E(x)] = F[w(x)F^{-1}[S(u)]]. \quad (18)$$

Ⅳ. Experimental Results

The 83-m, 330-element quasi-linear array operating at 9.6 GHz, having 3-m range resolution and 2-m cross-range resolution and producing 75 range bins, was used to image the nuclear power plant in Limerick, PA, USA, located 17.6 km from the array[11]. A basic ABF algorithm, called the DSA[8], was used for self-calibrating the large distorted phased array.

Beamforming bins having the normalized amplitude variance not larger than 0.12 have been shown to yield satisfactory images when the DSA is used for phase-cohering the array[5]. The relative effectiveness of 2-D imaging over 1-D imaging has been proved its usefulness to identify targets in the field of view even though the 2-D system requires more complicated signal processors[9].

A range bin 67 containing a specular-like beamformer of the normalized amplitude variance of 0.06 was selected for the ABF source. The phase measurements in this bin were used to compensate the phase errors of its own and the rest 74 bins. The corresponding image of the Limerick nuclear power plant is shown in Figure 2(a), which is used as the reference image $\hat{S}_1$ to calculate the correlation coefficient in (6). As the next beamforming bin, we take bin 29 having the amplitude variance of 0.07 which is a quite satisfactory beamformer since the variance is smaller than 0.12. Following the previous steps, we obtain another image $\hat{S}_2$, as shown in Figure 2(b). By comparing the two images shown in Figure 2, one can easily expect the higher value of the correlation coefficient. The correlation coefficient between the images is 0.980. For the remaining 73 bins, by consecutively selecting range bins as a test beamformer, we obtain 73 images corresponding to each bin and calculate the correlation coefficients with respect to the reference image $\hat{S}_1$. The image correlation coefficients of 0.9 or higher are shown in Figure 3 and also listed in Table 1. There are 12 range bins which produce the coefficients of 0.9 or higher. Figure 3 shows that the measured coefficients are all greater than the lower bound of the image correlation and the range bins having *rms* phase errors on the order of 30 degrees or less always guarantee the image correlation coefficients of 0.9 or higher.

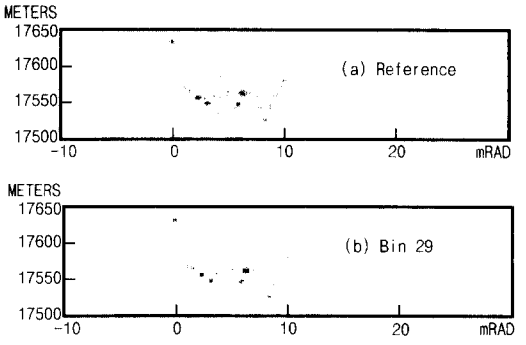

그림 2. Limerick 핵발전소의 range-azimuth 이미지 (a) 분산이 0.06 인 range bin을 사용하여 얻어진 이미지 (b) 분산이 0.07 인 range bin을 사용하여 얻어진 이미지

Fig. 2. Range-azimuth images of Limerick nuclear power plant. (a) Image obtained using range bin of the amplitude variance of 0.06. (b) Image obtained using range bin of the amplitude variance of 0.07.

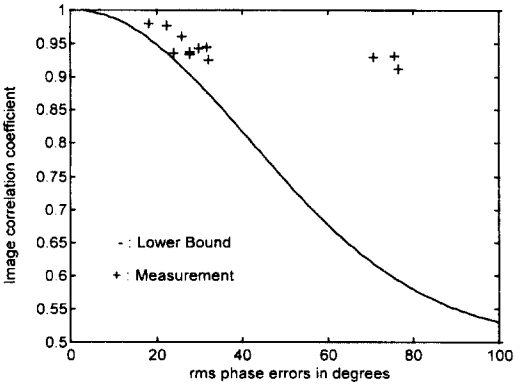

그림 3. Limerick 데이터를 사용한 이미지 코릴레이션 계수

Fig. 3. Image correlation measurements using Limerick data set.

V. Conclusions

We derived the theoretical relation between the phase-error variance and the image correlation coefficient indicating the degree of image degradation. The resultant relation was supported via implementing the image formation with real data where DSA was used as adaptive beamforming algorithm. It is expected that the relation can help select a suitable beamforming bin and

predict the corresponding output image even before the complicated image formation procedure. The authors wish to thank Dr. Steinberg of the University of Pennsylvania, USA, for providing the data for completion of this work.

표 1. 측정된 이미지 코릴레이션 계수
Table 1. Measured image correlation coefficients.

Range Bin Number	$\sigma_{\delta\phi}$	$\rho \geq 0.900$
7	27.82	0.937
8	22.45	0.977
10	70.68	0.930
11	75.61	0.931
28	29.81	0.943
29	18.32	0.980
31	27.60	0.934
32	23.98	0.935
51	32.15	0.925
55	25.94	0.961
56	31.60	0.944
66	76.39	0.912

$\sigma_{\delta\phi}$: the rms phase errors in degrees.
ρ : the image correlation coefficient.

References

[1] B.D. Steinberg, *Microwave Imaging with Large Antenna Arrays : Radio Camera Principles and Techniques*, John Wiley and Sons, New York, 1983.

[2] M.W. Long, *Radar Reflectivity of Land and Sea*, Artech House, Norwood, MA, 1983.

[3] N.C. Currie *et al.*, *Principles and Applications of Millimeter-Wave Radar*, Artech House, Norwood, MA, 1987.

[4] B.D. Steinberg, "Properties of Phase Synchronizing Sources for a Radio Camera," *IEEE Trans on Antennas and Propagation*, vol. AP-30, no. 6, pp. 1086-1092, Nov. 1982.

[5] B. Kang and S. Park, "Target-to-Clutter Ratio as a Measure of Beamformer Quality," 대한전자공학회, 하계종합학술대회논문집, 제20권, 제1호, pp. 187-190, 6월, 1997

[6] B.D. Steinberg, "A Theory of the Effect of Hard Limiting and Other Distortions upon the Quality of Microwave Images," *IEEE Trans. on Acoustics, Speech, and Signal Processing*, vol. ASSP-35, no. 10, pp. 1462-1472, Oct. 1987.

[7] J.B. Thomas, *An Introduction to Statistical Communication Theory*, John Wiley and Sons, New York, 1968.

[8] B. Kang, B.D. Steinberg, and S.B. Kesler, "A Solution for Self-Calibrating a Large Distorted Phased Array Using Subarray Processing," *IEEE Trans. on Antennas and Propagation*, vol. 39, no. 3, pp. 291-298, March 1991.

[9] B.D. Steinberg and B. Kang, "Relative Effectiveness of 2-D vs. 1-D High Resolution Microwave Imaging," *IEICE Proceedings of the International Symposium on Noise and Clutter Rejection in Radars and Imaging Sensors*, Kyoto, Japan, pp. 142-147, Nov. 1989.

저 자 소 개

姜 鳳 淳(正會員)

1962년 9월 27일생. 1985년 2월 연세대학교 전자공학과 졸업(공학사). 1987년 5월 펜실베니아대학원 전기과 졸업(공학석사). 1990년 8월 드렉셀대학원 전기전산학과 졸업(공학박사). 현재 (주)삼성전자 수석연구원. 주관심분야는 영상신호처리, 전파신호처리, 아날로그 회로설계 및 해석, VHDL/Verilog HDL Design Methodology 연구 등임

楊 勳 其(正會員) 第 34卷 D編 第 5號 參照